Spiral patterns in the anisotropy of acousto-optic figure of merit for LiNbO₃ crystals: The case of anisotropic diffraction in the interaction plane XY

Mys O., Kostyrko M., Krupych O. and Vlokh R.

Vlokh Institute of Physical Optics, 23 Dragomanov Street, 79005 Lviv, Ukraine, vlokh@ifo.lviv.ua

Abstract. We have analyzed the anisotropy of acousto-optic figure of merit (AOFM) in LiNbO₃ crystals for the three different types of anisotropic acousto-optic (AO) interactions associated with the interaction plane *XY*. The highest AOFM value $(6.4 \times 10^{-15}\,\text{s}^3/\text{kg})$ is reached for the type IX of anisotropic AO interactions. The highest AOFM for the collinear diffraction corresponds to the type VIII of AO interactions $(1.74 \times 10^{-15}\,\text{s}^3/\text{kg})$. We have found that the AOFM anisotropy in the *XY* plane is weak enough. With the exception of the collinear-diffraction region, it manifests spiral-like patterns.

Keywords: anisotropic acousto-optic diffraction, figure of merit, lithium niobate crystals

1. Introduction

Acousto-optic (AO) effect represents the basis underlying different optoelectronic devices for controlling laser radiation, e.g. modulators, deflectors, optical filters and radio-frequency spectral analyzers [1–4]. One of the most interesting cases of AO interactions is anisotropic AO diffraction. Perhaps, it has been described for the first time by R. W. Dixon as early as in the 1960s [5]. Different peculiarities of the anisotropic AO diffraction have been considered later on (see, e.g., Refs. [6–8]). Various geometries of the AO interactions and basic relations for the Bragg diffraction have been analyzed in Refs. [6, 7] for both optically uniaxial and biaxial crystals.

The authors of Ref. [6] have demonstrated that the diffraction occurring in the interaction plane perpendicular to the optic axis represents one of the specific geometries of AO interactions proper for optically uniaxial crystals. This geometry has proven to reveal a number of advantages and can, in principle, be recommended whenever optically uniaxial crystals are utilized as working elements of AO deflectors or collinear tunable AO filters. According to Ref. [6], the dependence of the Bragg angle Θ_B on the acoustic wave (AW) frequency is quadratic, with a maximum occurring at a certain AW frequency *f**. Note that, if compared with the standard case of isotropic AO interactions, the bandwidth of AO devices can be essentially extended around *f**, due to a weak dependence of Θ_B on the AW frequency f ($\left. \partial \Theta_B / \partial f \right|_{f=f*} = 0$) [4, 9]. According to Ref. [5], this property can be efficiently used in the AO deflectors based on the anisotropic diffraction, with no necessity in relying on cumbersome phased arrays of transducers. The same is true for the collinear tunable AO filters, which are operated using the uniaxial crystals and the AO interactions

that take place in the principal plane *XY*, where *X* and *Y* are the principal axes of the Fresnel ellipsoid in the plane perpendicular to the optic axis) [3].

It is worth noticing, however, that the effective elasto-optic coefficient (EEC) responsible for the AO diffraction, in particular for the collinear AO interactions, is usually rather small for the most of optically uniaxial crystalline materials (see, e.g., Ref. [4]). Indeed, when the AW propagates along the principal axes of the Fresnel ellipsoid and the conditions of the collinear diffraction hold true, the EEC is defined by the elasto-optic tensor components p_{41}, p_{45}, p_{46}, p_{52}, p_{54}, p_{56}, p_{63}, p_{64} and p_{65} [4]. One can easily notice that these coefficients become nonzero due to a symmetry lowering that occurs if one passes from some higher point symmetry groups (or Curie symmetry groups) to either trigonal (3m, 32, $\overline{3}$m, 3 and $\overline{3}$) or tetragonal (4, 4/m and $\overline{4}$), or hexagonal (6, 6/m and $\overline{6}$) groups. Hence, the coefficients mentioned deviate from zero only due to slight distortions of crystalline lattice and so they cannot be high enough.

On the other hand, it is known [4] that the requirement for the efficient collinear AO diffraction is $p_{ef} \geq 0.05$. As a result, in order to possibly achieve the efficient anisotropic AO interactions occurring in the *XY* plane, one should rely on essential anisotropy of the EEC and the AO figure of merit (AOFM) in this plane. In each case, this anisotropy deserves a thorough separate study. Recently we have developed a method for analyzing the anisotropy of both the AOFM and the EEC, which can be applied to the trigonal crystals belonging to the symmetry groups 3m, 32 and $\overline{3}$m [10, 11]. Moreover, the advantages of the method have been demonstrated on the example of LiNbO$_3$ crystals. To solve the problems described above, in the present work we apply this method to the analysis of anisotropy of the EEC and the AOFM to the specific case of AO interaction plane *XY* in the LiNbO$_3$ crystals.

2. Results and discussion

LiNbO$_3$ belongs to the point group 3m, for which one of the mirror symmetry planes is perpendicular to the crystallographic axis *a* [12], while the axis *c* is parallel to the three-fold symmetry axis. The crystallographic axes *a*, *b* and *c* correspond to the *X*, *Y* and *Z* axes of the Fresnel ellipsoid, respectively. The ordinary and extraordinary refractive indices are equal respectively to $n_o = 2.286$ and $n_e = 2.203$ [12]. In our further analysis, we also use the following quantitative data for the LiNbO$_3$ crystals: (i) the elasto-optic coefficients at $\lambda = 632.8$ nm are equal to $p_{11} = -0.023 \pm 0.017$, $p_{12} = 0.076 \pm 0.014$, $p_{13} = 0.147 \pm 0.019$, $p_{31} = 0.157 \pm 0.007$, $p_{33} = 0.141 \pm 0.013$, $p_{14} = 0.057 \pm 0.004$, $p_{41} = -0.051 \pm 0.011$ and $p_{44} = 0.126 \pm 0.004$ [13], (ii) the elastic stiffness coefficients at the constant electric field are as follows: $C_{11} = 2.03$, $C_{12} = 0.573$, $C_{13} = 0.752$, $C_{33} = 2.42$, $C_{44} = 0.595$, $C_{66} = 0.728$ and $C_{14} = 0.085$ (all in the units of 10^{11} N/m^2) [14], and (iii) the crystal density is $\rho = 4640$ kg/m^3 [14].

As shown in Ref. [11], the AOFM for the three possible types of anisotropic AO interactions are given by

$$M_2^{(VII)} = \frac{n_o^3 n *_e^3 \left\{ p_{ef}^{(VII)} \right\}^2}{\rho \left[v_{QL}(\chi, \varphi_X) \right]^3} , \quad M_2^{(VIII)} = \frac{n_o^3 n *_e^3 \left\{ p_{ef}^{(VIII)} \right\}^2}{\rho \left[v_{QT_1}(\chi, \varphi_X) \right]^3} , \quad M_2^{(IX)} = \frac{n_o^3 n *_e^3 \left\{ p_{ef}^{(IX)} \right\}^2}{\rho \left[v_{QT_2}(\chi, \varphi_X) \right]^3} , \quad (1)$$

where $v_{QL}(\chi, \varphi_X)$, $v_{QT_1}(\chi, \varphi_X)$ and $v_{QT_2}(\chi, \varphi_X)$ define the changes in the AW velocity occurring in the interaction plane *XZ* rotated around the *X* axis by the angle φ_X. Here

$$\chi = \arctan\left(\left|\frac{n_o \sin(\theta+\gamma) - n_o^* n_e \dfrac{\sin\theta}{\sqrt{n_o^{*2}\cos^2\theta + n_e^2\sin^2\theta}}}{n_o \cos(\theta+\gamma) - n_o^* n_e \dfrac{\cos\theta}{\sqrt{n_o^{*2}\cos^2\theta + n_e^2\sin^2\theta}}}\right|\right)\Bigg|_{\varphi_X=90\ \text{deg}}$$

$$= \arctan\frac{n_o \sin(\theta+\gamma) - n_e \sin\theta}{n_o \cos(\theta+\gamma) - n_e \cos\theta} \qquad (2)$$

is the orientation angle of the AW with respect to the X axis (see Fig. 1),

$$n_o^* = \frac{n_o n_e}{\sqrt{n_e^2 \cos^2\varphi_X + n_o^2 \sin^2\varphi_X}}\Bigg|_{\varphi_X=90\ \text{deg}} = n_e, \qquad (3)$$

$$n_e^* = \frac{n_o^* n_e}{\sqrt{(n_o^{*2}-n_e^2)\cos^2\varphi_X \sin^2\theta + n_e^2}}\Bigg|_{\varphi_X=90\ \text{deg}} = n_o^* = n_e, \qquad (4)$$

θ denotes the orientation angle of the incident optical wave vector with respect to the X axis and, finally, γ the angle between the diffracted optical wave vector and the wave vector of the incident optical wave. Let us remind that, in our notation, the types VII, VIII and IX describe the AO interactions with the quasi-longitudinal (QL) and the two quasi-transverse AWs (QT$_1$ and QT$_2$), respectively. Here the AW QT$_1$ is polarized in the interaction plane and the wave QT$_2$ perpendicular to this plane.
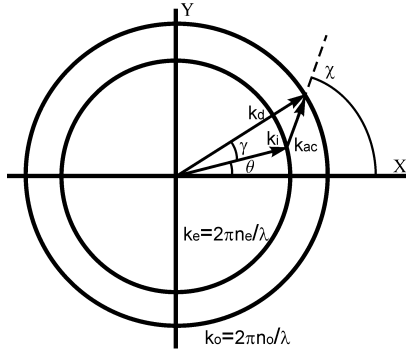

Fig. 1. Scheme of phase matching conditions corresponding to the AO interactions occurring in the principal plane XY: k_i, k_d and K_{ac} are the wave vectors of the incident optical wave, the diffracted optical wave and the AW, respectively.

As shown in our recent work [11], in the case of AO interactions of the type VII we deal with the rotation of the interaction plane around the X axis, so that the EEC is given by

$$p_{ef}^{(VII)} = \left\{ \begin{array}{l} -\left[p_{11}\cos^2\chi + p_{12}\sin^2\chi\sin^2\varphi_X + p_{13}\sin^2\chi\cos^2\varphi_X + p_{14}\sin 2\varphi_X\sin^2\chi\right]\times \\[4pt] \times\sqrt{1 - \dfrac{\sin\theta\sin\varphi_X}{\sqrt{1-\sin^2\theta\cos^2\varphi_X}}}\,\sin\theta\cos\varphi_X - \\[12pt] -\left[p_{66}\sin 2\chi\sin\varphi_X + p_{14}\sin 2\chi\cos\varphi_X\right]\dfrac{\sin\theta\sin\varphi_X}{\sqrt{1-\sin^2\theta\cos^2\varphi_X}}\sin\theta\cos\varphi_X + \\[12pt] +\left[p_{44}\sin 2\chi\cos\varphi_X + p_{41}\sin 2\chi\sin\varphi_X\right]\sqrt{1-\sin^2\theta\cos^2\varphi_X} \end{array} \right\} \times$$

$$\times\left(\frac{\sin(\theta+\gamma)\sin\varphi_X}{\sqrt{1-\sin^2(\theta+\gamma)\cos^2\varphi_X}}\right) -$$

$$-\left\{\begin{array}{l}-\left[p_{66}\sin 2\chi \sin\varphi_X + p_{14}\sin 2\chi \cos\varphi_X\right]\sqrt{1-\dfrac{\sin\theta \sin\varphi_X}{\sqrt{1-\sin^2\theta \cos^2\varphi_X}}}\sin\theta \cos\varphi_X - \\[4mm] -\left[p_{12}\cos^2\chi + p_{11}\sin^2\chi \sin^2\varphi_X + p_{13}\sin^2\chi \cos^2\varphi_X - p_{14}\sin 2\varphi_X \sin^2\chi\right]\times \\[2mm] \times \dfrac{\sin\theta \sin\varphi_X}{\sqrt{1-\sin^2\theta \cos^2\varphi_X}}\sin\theta \cos\varphi_X + \\[4mm] +\left[p_{44}\sin^2\chi \sin 2\varphi_X + p_{41}(\cos^2\chi - \sin^2\chi \sin^2\varphi_X)\right]\sqrt{1-\sin^2\theta \cos^2\varphi_X}\end{array}\right\}\times$$

$$\times\sqrt{1-\dfrac{\sin^2(\theta+\gamma)\sin^2\varphi_X}{1-\sin^2(\theta+\gamma)\cos^2\varphi_X}}. \tag{5}$$

Under the condition $\varphi_X = 90$ deg (i.e., for the AO interactions in the *XY* plane) Eq. (5) can be rewritten as

$$p_{ef}^{(VII)} = p_{41}\left(\sin 2\chi \sin(\theta+\gamma) - \cos 2\chi \cos(\theta+\gamma)\right). \tag{6}$$

As seen from Eq. (6), the EEC for this interaction plane is given by a single elasto-optic tensor component, p_{41} ($|p_{41}| = 0.051 \pm 0.011$ [13] – see above). Moreover, both the slowness of the longitudinal AW (see Fig. 2e) and the refractive indices of the optical waves do not depend upon the angle $\theta+\gamma$. Nonetheless, the AOMF in the interaction plane *XY* depends on the incident and diffraction angles, due to appropriate dependence of the EEC (see Fig. 2b, d). As a consequence, the AOFM manifests a spiral-like dependence on the angle $\theta+\gamma$.

The maximum AOFM, which can be reached for this AO interaction type, is equal to 0.25×10^{-15} s^3/kg (see Fig. 2a, c). This AOFM value occurs at $\theta = 0$ (or 180 deg) for the case of collinear diffraction as well as at all the other diffraction angles in the case of usual anisotropic AO interaction.

When the type VIII of AO interactions with the AW QT$_1$ is dealt with (i.e., the case of rotation of the interaction plane around the *X* axis), the EEC becomes as follows [11]:

$$p_{ef}^{(VIII)} = \left\{\begin{array}{l}-0.5\left[p_{11} - p_{12}\sin^2\varphi_X - p_{13}\cos^2\varphi_X - p_{14}\sin 2\varphi_X\right]\times \\[2mm] \times\sin 2\chi\sqrt{1-\dfrac{\sin\theta \sin\varphi_X}{\sqrt{1-\sin^2\theta \cos^2\varphi_X}}}\sin\theta \cos\varphi_X - \\[4mm] -\left[p_{66}\sin\varphi_X + p_{14}\cos\varphi_X\right]\cos 2\chi \dfrac{\sin\theta \sin\varphi_X}{\sqrt{1-\sin^2\theta \cos^2\varphi_X}}\sin\theta \cos\varphi_X + \\[4mm] +\left[p_{44}\cos\varphi_X + p_{41}\sin\varphi_X\right]\cos 2\chi\sqrt{1-\sin^2\theta \cos^2\varphi_X}\end{array}\right\}\times$$

$$\times\left(\dfrac{\sin(\theta+\gamma)\sin\varphi_X}{\sqrt{1-\sin^2(\theta+\gamma)\cos^2\varphi_X}}\right) \tag{7}$$

$$-\left\{\begin{array}{l}-\left[p_{66}\sin\varphi_X + p_{14}\cos\varphi_X\right]\cos 2\chi\sqrt{1-\dfrac{\sin\theta \sin\varphi_X}{\sqrt{1-\sin^2\theta \cos^2\varphi_X}}}\sin\theta \cos\varphi_X - \\[4mm] -0.5\left[p_{12} - p_{11}\sin^2\varphi_X - p_{13}\cos^2\varphi_X + p_{14}\sin 2\varphi_X\right]\times \\[2mm] \times\sin 2\chi \dfrac{\sin\theta \sin\varphi_X}{\sqrt{1-\sin^2\theta \cos^2\varphi_X}}\sin\theta \cos\varphi_X + \\[4mm] +0.5\left[-p_{44}\sin 2\varphi_X + p_{41}(1+\sin^2\varphi_X)\right]\sin 2\chi \times\sqrt{1-\sin^2\theta \cos^2\varphi_X}\end{array}\right\}\times$$

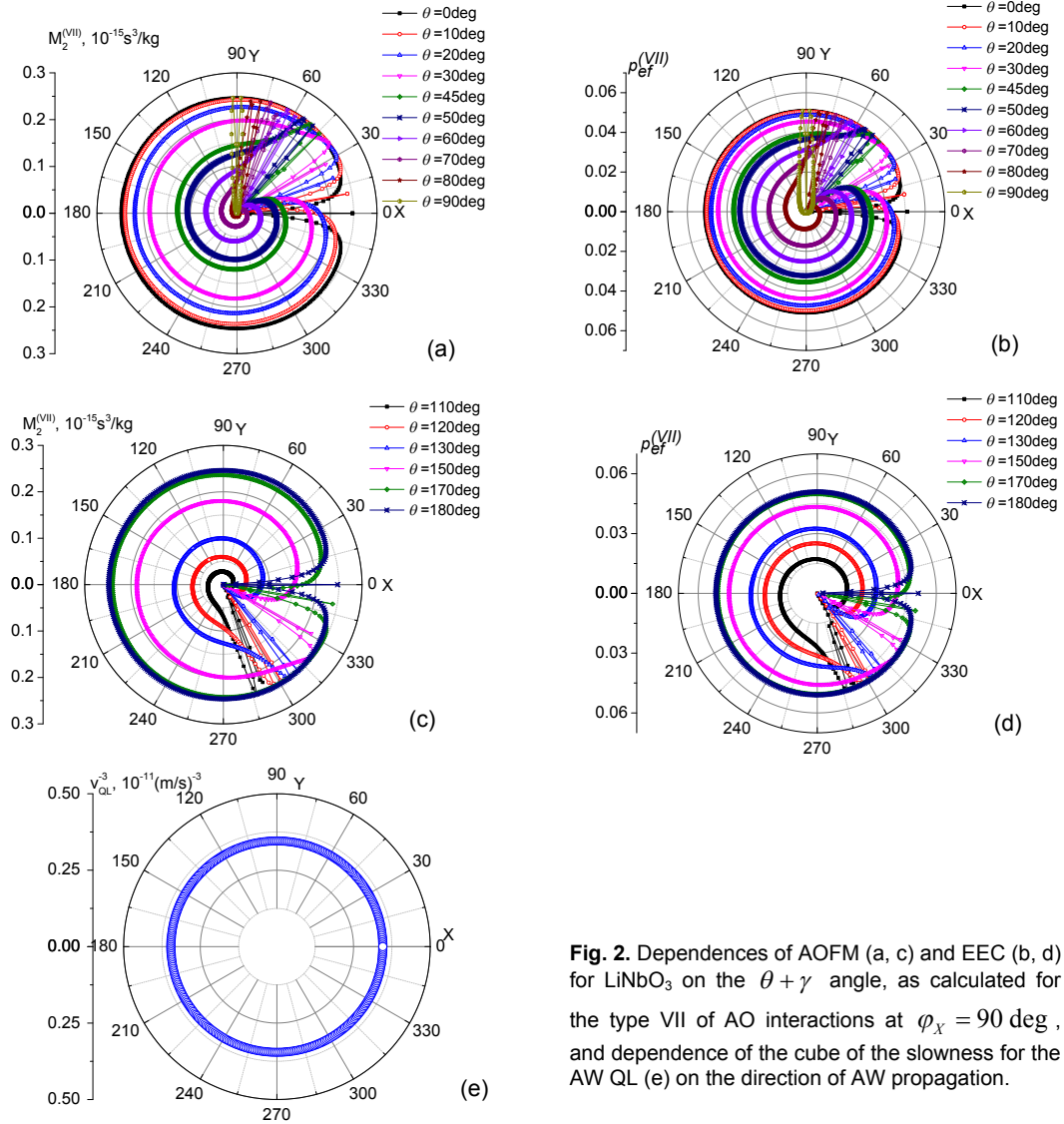$$\times\sqrt{1-\dfrac{\sin^2(\theta+\gamma)\sin^2\varphi_X}{1-\sin^2(\theta+\gamma)\cos^2\varphi_X}}.$$

Fig. 2. Dependences of AOFM (a, c) and EEC (b, d) for LiNbO$_3$ on the $\theta + \gamma$ angle, as calculated for the type VII of AO interactions at $\varphi_X = 90 \deg$, and dependence of the cube of the slowness for the AW QL (e) on the direction of AW propagation.

Under the condition $\varphi_X = 90 \deg$ Eq. (7) simplifies to

$$p_{ef}^{(VIII)} = p_{41}\left(\cos 2\chi \sin(\theta + \gamma) - \sin 2\chi \cos(\theta + \gamma)\right), \tag{8}$$

i.e. the EEC is determined by the same elasto-optic coefficient as for the type VII of AO diffraction, and by the similar analytical relation. However, due to higher slownesses peculiar for the AW QT$_1$ (see Fig. 3e), the AOFM for the interaction type VIII is higher when compared with the type VII considered above. For example, the highest AOFM value possible for the interaction type VIII is equal to 1.74×10^{-15} s^3/kg. This AOFM is reached with the collinear diffraction at $\theta = 90$. (Notice that the forward collinear diffraction is realized at $\gamma = 0$, while the backward collinear diffraction occurs at $\gamma = 180 \deg$ [15]).

A narrow peak detected in our recent work [16], which appears under the condition $\gamma = 0$ in the interaction plane ZX, can also exist in the XY plane. It occurs at $0 \deg < \theta < 90 \deg$ for the case

of forward collinear diffraction and at $90 \deg < \theta < 180 \deg$ for the backward diffraction (see Fig. 3a, c). Notice also that the same AOFM value is reached at the usual anisotropic diffraction and the condition $\theta = 90 \deg$ for some other values of the γ angle. On the other hand, two rather narrow AOFM maximums are observed at $\theta = 0$. They are symmetrical with respect to the X axis and, at $\gamma = \pm 2 \deg$, the AOFM for the anisotropic diffraction is equal to $1.73 \times 10^{-15} \text{ s}^3/\text{kg}$ (see Fig. 3a). As seen from Fig. 3e, a hexagonal-like distortion of the shape of the AOFM is caused by the same distortion occurring with the cross section of the AW slowness surface. The two-dimensional EEC and AOFM curves manifest spiral-like shapes, although there are some deviations from this 'spiral' behaviour in the region of the collinear AO diffraction.
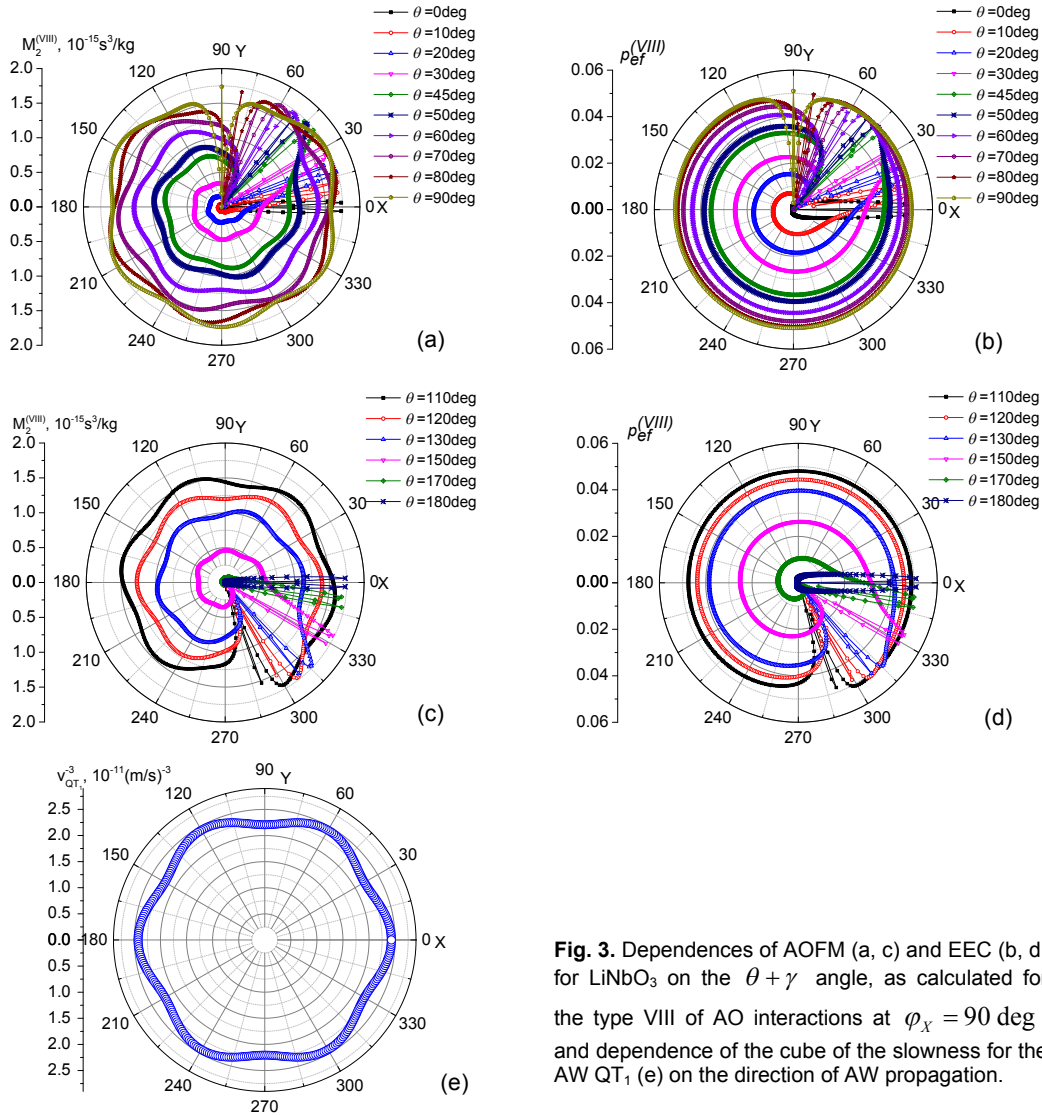

Fig. 3. Dependences of AOFM (a, c) and EEC (b, d) for LiNbO$_3$ on the $\theta + \gamma$ angle, as calculated for the type VIII of AO interactions at $\varphi_X = 90 \deg$, and dependence of the cube of the slowness for the AW QT$_1$ (e) on the direction of AW propagation.

Now we proceed to the type IX of AO interactions with the AW QT$_2$. This wave is polarized perpendicular to the interaction plane, i.e. the latter plane is rotated around the X axis. The EEC is given by the relation [11]

$$
p_{ef}^{(IX)} = \left\{
\begin{array}{l}
-\left[(-p_{12}+p_{13})\sin\chi\sin 2\varphi_X - p_{14}\sin\chi\cos 2\varphi_X\right]\sqrt{1-\dfrac{\sin\theta\sin\varphi_X}{\sqrt{1-\sin^2\theta\cos^2\varphi_X}}}\sin\theta\cos\varphi_X - \\[4mm]
-\left[p_{66}\cos\varphi_X - p_{14}\sin\varphi_X\right]\cos\chi\,\dfrac{\sin\theta\sin\varphi_X}{\sqrt{1-\sin^2\theta\cos^2\varphi_X}}\sin\theta\cos\varphi_X + \\[4mm]
+\left[-p_{44}\sin\varphi_X + p_{41}\cos\varphi_X\right]\cos\chi\sqrt{1-\sin^2\theta\cos^2\varphi_X}
\end{array}
\right\} \times
$$

$$
\times\left(\frac{\sin(\theta+\gamma)\sin\varphi_X}{\sqrt{1-\sin^2(\theta+\gamma)\cos^2\varphi_X}}\right)
$$

$$
-\left\{
\begin{array}{l}
-\left[p_{66}\cos\varphi_X - p_{14}\sin\varphi_X\right]\cos\chi\sqrt{1-\dfrac{\sin\theta\sin\varphi_X}{\sqrt{1-\sin^2\theta\cos^2\varphi_X}}}\sin\theta\cos\varphi_X - \\[4mm]
-\left[(-p_{11}+p_{13})\sin\chi\sin 2\varphi_X + p_{14}\sin\chi\cos 2\varphi_X\right]\dfrac{\sin\theta\sin\varphi_X}{\sqrt{1-\sin^2\theta\cos^2\varphi_X}}\sin\theta\cos\varphi_X + \\[4mm]
+\left[-p_{44}\cos 2\varphi_X - p_{41}\sin 2\varphi_X)\right]\sin\chi\times\sqrt{1-\sin^2\theta\cos^2\varphi_X}
\end{array}
\right\} \times
$$

$$
\times\sqrt{1-\frac{\sin^2(\theta+\gamma)\sin^2\varphi_X}{1-\sin^2(\theta+\gamma)\cos^2\varphi_X}}. \tag{9}
$$

For the interaction plane XY ($\varphi_X = 90\deg$) Eq. (9) reads as

$$
p_{ef}^{(IX)} = p_{44}\left(\sin\chi\cos(\theta+\gamma) - \cos\chi\sin(\theta+\gamma)\right), \tag{10}
$$

where $p_{44} = 0.126 \pm 0.004$ [13], as mentioned before. It is readily seen from Eq. (10) that $p_{ef}^{(IX)} = 0$ under the conditions of collinear AO diffraction (i.e., at $\gamma = 0$ and $\theta = \chi$). Hence, the collinear diffraction is forbidden for the type IX of AO interactions. However, the anisotropic AO interaction is still possible at some other diffraction angles. The EEC curves are the same for different θ angles (see Fig. 4b, d) and the AOFM curves remain almost the same (see Fig. 4a, c), being only slightly distorted by the anisotropy of the AW slowness (see Fig. 4e). These curves rotate in the same way with changing θ angle. The maximum AOFM value (6.4×10^{-15} s^3/kg) is reached at $\gamma \simeq \pm 23\deg$, which corresponds to the AW frequency $f = 5.65$ GHz (see Fig. 4). This is the highest AOFM possible in the case of anisotropic AO diffraction occurring in the XY plane of LiNbO$_3$.

Following from the results reported above, one concludes that the type IX of AO interactions in the XY plane can be used for non-collinear tunable AO filtering with LiNbO$_3$ crystal as a working element. At the collinear geometry of anisotropic AO diffraction, the types VII and VIII of AO interactions should be suitable for the same aim.

3. Conclusions

In the present work we have analyzed the anisotropy of the AOFM in LiNbO$_3$ for the three different types of anisotropic AO interactions that occur in the principal interaction plane XY. We have found that the type VII of AO interactions with the longitudinal AW results in the AOFM, which is determined by the elasto-optic coefficient p_{41} and remains comparatively small (0.25×10^{-15} s^3/kg). In case of the type VIII of AO interactions with the AW QT$_1$, the AOFM is determined by the same elasto-optic coefficient and its highest value is equal to 1.74×10^{-15} s^3/kg.

Both of the AO interaction types mentioned above can be realized either in collinear or non-collinear geometries of the anisotropic diffraction. The third case considered in this work is the type IX of AO interactions with the AW QT_2 polarized perpendicular to the XY plane. Then the collinear AO diffraction is impossible, though the usual anisotropic diffraction still can take place. The highest AOFM for the anisotropic diffraction in the interaction plane XY amounts to 6.4×10^{-15} s^3/kg.
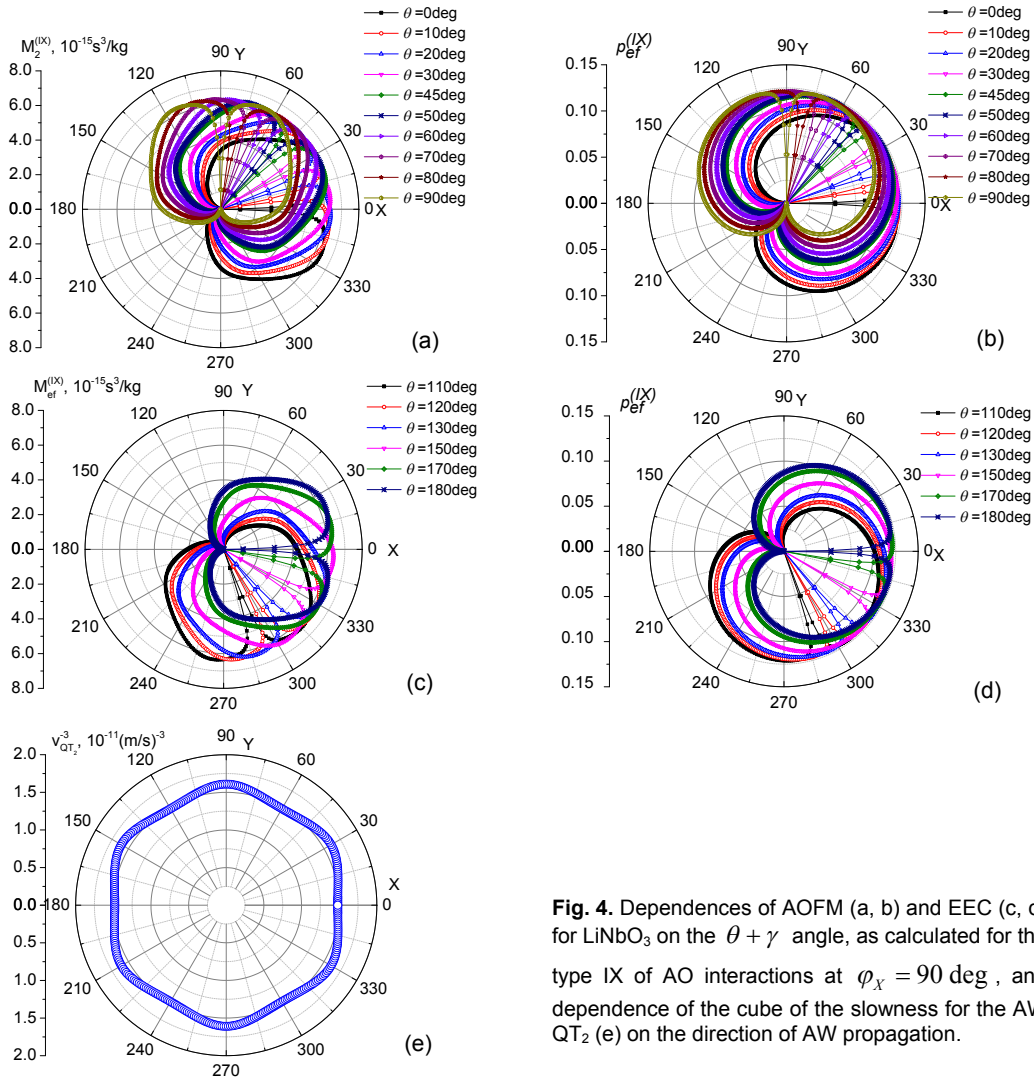

Fig. 4. Dependences of AOFM (a, b) and EEC (c, d) for LiNbO$_3$ on the $\theta + \gamma$ angle, as calculated for the type IX of AO interactions at $\varphi_X = 90$ deg, and dependence of the cube of the slowness for the AW QT_2 (e) on the direction of AW propagation.

The maximal AOFM typical for the collinear AO interactions in the XY plane is equal to 1.74×10^{-15} s^3/kg. This value corresponds to the type XIII of AO interactions and is reached at $\theta = 90$ deg, i.e. under conditions when the three interacting waves propagate along the Y axis. As a consequence, the type IX of AO interactions that occur in the XY plane can be utilized in the wide-band non-collinear tunable AO filters built on the LiNbO$_3$ crystals as working elements. The types VII and VIII of AO interactions are suitable for the same aim with the collinear geometries of anisotropic diffraction. Finally, the AOFM anisotropy in the XY plane of LiNbO$_3$ appears to be rather weak. It is also interesting that the above anisotropy manifests spiral-like patterns, except for a small region of the collinear AO interactions.

8

Ukr. J. Phys. Opt. 2016, Volume 17, Issue 1

References

1. Chang I C, Acousto-optic devices and applications, in M. Bass, E. S. Van Stryland, D. R. Williams, and W L. Wolfe, Handbook of optics, vol. II, Devices, measurement and properties, New York: McGraw-Hill, Chapter 12, pp.12.1–12.54.
2. Korpel A, Acousto-optics, 2nd Ed. New York: Marcel Dekker, Inc (1997).
3. Magdich L N and Molchanov V Ya, Acoustooptic devices and their application, Moscow: "Sovetskoe Radio" (1978).
4. Balakshiy V I, Parygin V N and Chirkov L E, Physical basis of acoustooptics, Moscow: "Radio i Svyaz" (1985).
5. Dixon R W, 1967. Acoustic diffraction of light in anisotropic media. IEEE J. Quant. Electr. **3**: 85—93.
6. Lemanov V V and Shakin O V, 1972. Light scattering on the elastic waves in uniaxial crystals. Fiz. Tverd. Tela. **14**: 229–236.
7. Pisarevsky Yu V and Silvestrova I M, 1973. Light scattering on the elastic waves in optically biaxial crystals. Kristallografiya. **18**: 1003–1013.
8. Parygin V N and Chirkov L E, 1975. Light diffraction by the ultrasound in anisotropic media. Kvant. Electron. **2**: 318–326.
9. Balakshiy V I, Voloshinov V B and Parygin V N, 1971. Acoustic scanning by light in anisotropic media. Radiotechn. Elektron. **16**: 2226–2229.
10. Mys O, Kostyrko M, Krupych O and Vlokh R, 2015. Anisotropy of the acoustooptic figure of merit for LiNbO$_3$ crystals: isotropic diffraction. Appl. Opt. **54**: 8176–8186.
11. Mys O, Kostyrko M and Vlokh R, 2015. The anisotropy of acousto-optic figure of merit for LiNbO$_3$ crystals: Anisotropic diffraction. Appl. Opt. (to be published).
12. Weis R S and Gaylord T K. 1985. Lithium niobate: summary of physical properties and crystal structure. Appl. Phys. A. **37**: 191–203.
13. Krupych O, Savaryn V and Vlokh R, 2014. Precise determination of full matrix of piezo-optic coefficients with a four-point bending technique: the example of lithium niobate crystals. Appl. Opt. **53**: B1–B7.
14. Smith R T and Welsh F S, 1971. Temperature dependence of the elastic, piezoelectric, and dielectric constants of lithium tantalate and lithium niobate. J. Appl. Phys. **42**: 2219–2230.
15. Jose E B Oliveira and Cheng-Kuei Jen, 1990. Backward collinear acoustooptic interactions in bulk materials. Appl. Opt. **29**: 836–840.
16. Mys O, Kostyrko M, Vasylkiv Yu and Vlokh R, 2015. Anomalous behaviour of acoustooptic figure of merit under the conditions of collinear diffraction. Ukr. J. Phys. Opt. **16**: 187-192.

Анотація. Проаналізовано анізотропію коефіцієнта акустооптичної якості кристалів LiNbO$_3$ для трьох типів анізотропної акустооптичної (АО) дифракції в площині взаємодії XY. Коефіцієнт акустооптичної якості досягає найвищого значення (6,4×10^{-15} с^3/кг) у випадку анізотропної дифракції для типу IX АО взаємодії. Найвище значення у разі колінеарної дифракції властиве для типу VIII АО взаємодії (1,74×10^{-15} с^3/кг). Виявлено, що анізотропія коефіцієнта акустооптичної якості в площині XY кристалів LiNbO$_3$ слабка і, за винятком області колінеарної дифракції, виявляє спіралевидну поведінку.